





Millijoule few-cycle pulses from staged compression for strong and high field science

M. STANFIELD,^{1,*} N. F. BEIER,¹ S. HAKIMI,^{1,2}  H. ALLISON,¹ D. FARINELLA,¹  A. E. HUSSEIN,^{1,3} T. TAJIMA,¹ AND F. DOLLAR¹

¹*STROBE, NSF Science & Technology Center, Dept. of Physics & Astronomy, University of California, Irvine, Irvine, CA 92697, USA*

²*Present address: Lawrence Berkeley National Laboratory, Berkeley, CA 94720, USA*

³*Present address: University of Alberta, Department of Electrical and Computer Engineering, Edmonton, AB, T6G 2W3, Canada*

*stanfem@uci.edu

Abstract: Intense few-cycle laser pulses have a breadth of applications in high energy density science, including particle acceleration and x-ray generation. Multi-amplifier laser system pulses have durations of tens of femtoseconds or longer. To achieve high intensities at the single-cycle limit, a robust and efficient post-compression scheme is required. We demonstrate a staged compression technique using self-phase modulation in thin dielectric media, in which few-cycle pulses can be produced. The few-cycle pulse is then used to generate extreme ultraviolet light via high harmonic generation at strong field intensities and to generate MeV electron beams via laser solid interactions at relativistic intensities.

© 2021 Optical Society of America under the terms of the [OSA Open Access Publishing Agreement](#)

1. Introduction

Since the advent of Chirped Pulse Amplification [1], a rapid increase of focused laser intensity has occurred, to the current record of $5.5 \times 10^{22} \text{ Wcm}^{-2}$ [2]. Relativistic intensities, $> 10^{18} \text{ Wcm}^{-2}$ at wavelengths of $\lambda \approx 1 \mu\text{m}$, enable applications from compact GeV electron acceleration via Laser Wakefield Acceleration (LWFA) [3–6] to MeV photon generation via laser-Compton scattering [7,8]. Few-cycle intense lasers enable access to new regimes of science. Recent simulations suggest that a dramatic improvements in proton energy spread and maximum energy can be achieved as pulse durations approach a single cycle [9], while the production of multi-MeV energy electron beams from LWFA have been demonstrated using few-cycle laser pulses at kilohertz repetition rates with only a few millijoules of laser energy [10–14]. Additionally, the use of few-cycle laser pulses enable efficient generation of attosecond pulses via relativistic high harmonic generation [15,16].

Due to inherent limitations of amplification, pulse durations are typically on the order of tens of femtoseconds (fs), or ≈ 10 laser cycles at 800 nm. Post-compression is a technique in which the output of a laser system is spectrally broadened, and then phase corrected to produce pulses with shorter pulse durations. The spectral broadening is most commonly performed via Kerr-induced self-phase modulation (SPM), which was demonstrated several decades ago using optical fibers as the nonlinear medium [17,18]. In general, SPM is used to generate broadened spectra, which then enables a shorter transform-limited pulse duration. If the SPM medium is unable to compensate for spectral phase differences (e.g., dispersion effects), then dispersion correcting optics such as chirped mirrors may be used. Since these early experiments, many techniques of post-compression have been developed.

For pulses which have durations initially on the order of picoseconds or longer, considerable bandwidth must be generated. To achieve such large amounts of nonlinearity, there necessarily must be large amounts of propagation through the SPM medium, as increasing intensity leads to optical damage. One important consideration for SPM is the accumulation of wavefront errors, as

small intensity modulations can be enhanced and self-focused, often leading to the catastrophic degradation of the laser wavefront [19]. Techniques such as multi-pass cells [20–22] ensure beam quality by placing the SPM medium inside of a cavity. While this method has been shown to support laser energies up to hundreds of mJ [20], reducing the final pulse duration below a limit of tens of femtoseconds is difficult due to effects such as optical wave breaking [21].

Pulse compression to single or few optical cycles can be achieved by using laser pulses which are initially tens to hundreds of femtoseconds. Higher intensities can be achieved with much lower energy, and the factor of spectral broadening required is smaller than for picosecond pulse lasers. For these pulses, the SPM medium can be placed at the focus to enable efficient SPM. Microjoules of laser energy compression has been demonstrated by propagating through a bulk dielectric, and the portion of the beam with the most pulse broadening can be discriminated for use in experiment [23–26]. At higher laser energies, the small and large scale self focusing prevents the bulk from being used as an SPM medium. A popular technique to compress laser pulses is hollow core fiber compression, in which the laser is focused into a hollow-core, gas filled waveguide which acts as the SPM medium [27]. Though this technique has been shown to work up to pulse energies of millijoules [28,29], waveguides on the order of meters in length are required and must have a sufficiently large diameter to prevent substantial ionization of the gas inside the fiber [29]. Furthermore, losses are typically on the order of 35-50% [28,30–32]. Scaling hollow core fiber compression to even higher intensities is thus practically difficult. Another technique known as multiple plate compression utilizes cascading dielectric plates [33,34]. Placing a plate near the laser focus enables a strong nonlinear lens to occur, which then provides a waveguiding effect through the multiple plates. While this technique has also been shown to accommodate up to a millijoule of laser energy [35], the geometry would have to be scaled considerably to maintain the correct nonlinear lensing geometry for significantly higher pulse energies.

A technique that has been proposed to produce few-cycle laser pulses that is scalable to Joule energy levels is Thin-film Compression (TFC) [36,37]. In TFC, a collimated, top-hat beam profile is spectrally broadened through a thin dielectric film. The thin films can be various amorphous materials, for instance, a variety of glasses and plastics have been used in the past [38–44]. While TFC has been used to compress pulses up to a factor of 5 on multi-Joule systems [45,46], relativistic intensities have only been produced with tens of femtosecond pulse durations [41,47]. In order to achieve uniform broadening, a top-hat beam profile is necessary, and the collimated geometry of the large beam diameters produce negligible nonlinear lensing effects. For the common Gaussian beam profile, spatially varying phase causes the focal spot quality to be strongly diminished [40,47]. TFC has been staged to achieve higher compression, as proposed in [36] and implemented in [48], has numerous benefits [40]. One major benefit is the additional distance between the plates can enable self-healing of the beam to occur, mitigating effects of beam breakup [49] for TFC and multiple plate compression.

In this Article, we demonstrate a stageable pulse compression scheme using thin dielectric media to produce high intensity, few-cycle pulses suitable for strong and high field science applications. A spectral broadening factor up 6.8 was shown for three stages. The output of two stages was compressed to a measured 7 femtoseconds, and the focal spot was shown to be minimally affected by wavefront errors. This beam was used to generate broadened harmonic spectrum in a high harmonic generation experiment, and MeV electrons from a relativistically intense laser solid interaction.

2. Experimental setup

The experiments were performed using a commercially available, single-stage Ti:Sapphire regenerative amplifier (Spectra-Physics Solstice ACE) operating at a kilohertz repetition rate with a central wavelength of 800 nm with P-polarization. The wavefront was a Gaussian mode with

an M^2 of <1.25 . The initial pulse duration was measured to be 36 fs as measured by a second harmonic generation frequency resolved optical gating (SHG FROG) with a 70 nm bandwidth at the -20 dB level. The laser energy delivered at the input of the compression set-up was up to 6.9 millijoules, corresponding to a maximum peak power of 180 GW, though for most experiments 0.95 mJ was used to prevent optical damage. The energy throughput depends on the number of stages used and is limited by the reflectivity of the mirrors used. For example, the energy throughput of the two stage system is $75\pm 1\%$, primarily from the use of metallic mirrors.

We used a two stage pulse compression scheme for most of the characterization and experiments in this paper, as shown in Fig. 1. The laser enters a reflective Galilean telescope consisting of two curved mirrors, which relays the beam through focus. A thin plate of fused silica is placed sufficiently far from focus such that ionization of the material is suppressed, yet close enough such that nonlinearity is present. In all experiments presented here, we placed the fused silica such that the intensity on target is approximately 4 TWcm^{-2} . Fused silica plates were used due to the high damage threshold, optical quality, and known optical parameters. The laser intensity in the fused silica can be adjusted by positioning the plates at a suitable location along the optical axis. The pulse compression apparatus is housed inside a vacuum chamber, to enable the laser to pass through focus without laser breakdown occurring.

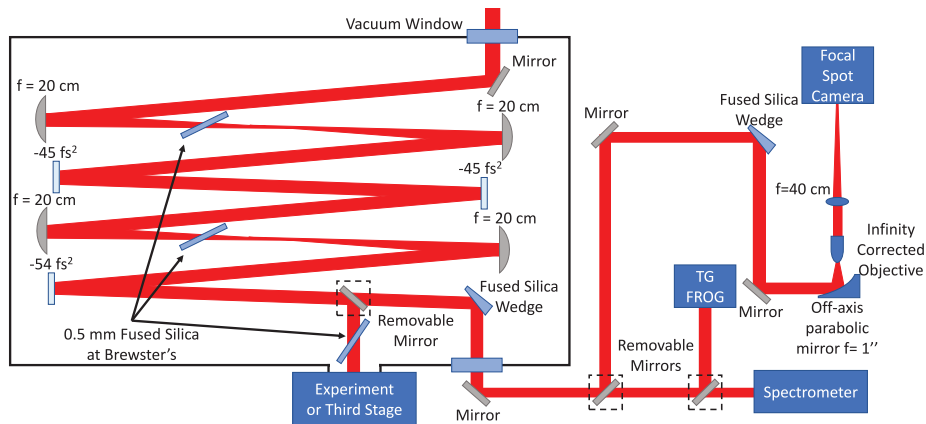


Fig. 1. Two Stage Experimental Setup The pulse enters at the top and is directed into the first stage reflective telescope, consisting of two curved mirrors. Spectra broadening occurs inside of a 0.5 mm fused silica plate oriented at Brewster's angle. The collimating curved mirror in each stage is positioned to collimate the broadened beam which experiences nonlinear lensing. The beam can be sent into an additional stage, into an experiment, or into characterization diagnostics. The power is reduced for the characterization diagnostics by multiple reflections off of wedged glass substrates.

A single $500 \mu\text{m}$ thick fused silica plate is used as the SPM media in each stage. The plates were positioned at Brewster's angle to minimize reflection losses, increasing the propagation length to $600 \mu\text{m}$. Due to the small beam size on the fused silica plate, Kerr lensing of the broadened beam is non-negligible, which shifts the focus closer to the focusing optic of the telescope [40]. The collimation optic is placed to compensate this nonlinear lensing, outputting a collimated, broadened pulse and reducing the overall length of the telescope. The residual unbroadened laser pulse, not experiencing the nonlinear lens, will output the telescope with positive divergence. For high efficiency compression to occur, pulses are recompressed between stages, which is done with commercially available chirped mirrors (Newport 10Q20UF.40 and Thorlabs UMC10-15FS) as the dispersion compensating optics.

To temporally characterize the broadened beam without introducing additional nonlinearities, the beam was reduced in intensity by reflecting off fused silica wedges near Brewster's angle. Temporal characterization of this pulse was performed by sending the beam into a transient-grating frequency resolved optical gating (TG-FROG) due to the supercontinuum nature of the pulse. The beam can be diverted from the TG-FROG into a $F/2$ off-axis parabolic (OAP) mirror to characterize the focal spot. The focal spot was reimaged using an infinity-corrected, plane achromatic microscope objective and an imaging lens which magnified the focal spot onto a digital camera. The wavelength dependence of the far field was measured by placing dielectric bandpass filters (Thorlabs FB650-40, Newport 10BPF10-700, and Thorlabs FB800-10) in the collimated portion of the focal spot imaging optics. The diagnostics were aligned with the collimated, many cycle laser output. The broadened output of the pulse compressor was aligned into the diagnostics without changing any of the imaging conditions. While imaging the broadened beam, any residual portion of the unbroadened beam will not be properly collimated and thus is focused to a different focal plane in both the TG-FROG and the focal spot characterization setup.

The broadened spectrum is measured by taking a spatial average of the beam, either by measuring diffuse scatter of the beam onto a screen, or by focusing the beam onto a cosine corrector and optical fiber spectrometer. Both measurements produced similar results, and the spectrometer was calibrated with a NIST-calibrated Tungsten Halogen lamp. When possible, the entire beam was used for diagnostics and characterization. However, the diverging unbroadened portion of the beam, preferentially existing in the outer edge of the beam, was blocked by a hard aperture in the TG-FROG and in the third stage spectral measurements.

3. Results

3.1. Spectral broadening numerical modeling

Numerical modeling of the interaction was performed using a Python nonlinear optics package (PyNLO). PyNLO solves the generalized nonlinear Schrodinger equation using a split-step Fourier method (SSFM) [50,51]. Though including self-steepening and the delayed Raman response in the simulations produced better agreement with experiment, inclusion of material dispersion has the largest effect. Material dispersion was modeled up to the fourth order dispersion term of fused silica. The thickness of material and locations of the fused silica were the same as the experimental values. Before each stage, the reflective losses from two silver mirrors (Newport ER.2) are taken into account. Due to the target being oriented at Brewster's angle to minimize reflective losses, there is an effective decrease of the peak intensity of ~ 1.4 within the fused silica. The initial pulse for the simulation matches the experiment with a measurement taken with a SHG-FROG and includes simulating the nonlinear propagation in air and the vacuum window.

The simulations are one dimensional, though unexpectedly produce predicted spectra consistent with experimental measurements. This is because the the areas of highest intensity will produce the most bandwidth, and in a spatially integrated spectrum the extrema of the spectra are from this central portion. While two dimensional simulations would undoubtedly produce better agreements, we experimentally observe consistent enough correlation between experiment and simulation that such an approach was not warranted.

Though the targets are thin, introducing a small amount of group delay dispersion (GDD) induced from material dispersion will dramatically alter the SPM modulated output spectrum; we observed a predicted FTL pulse duration 40% shorter than experimentally measured for the 2 stage system when not including dispersion. Asymmetric broadening is observed in both simulated and experimental results, largely due to the residual third-order phase inherent to many laser systems. Material dispersion, self-steepening, delayed Raman response also contributing to the asymmetric broadening of the spectrum.

3.2. Experimental compression

The numerical modeling was used to determine the intensity on the dielectric plates, and the magnitude of dispersion correction required for the chirped mirrors. Placing the fused silica plates to produce the expected intensities, the laser bandwidth is nearly tripled to 198 nm maintaining the central wavelength of 800 nm, corresponding to an FTL duration of 12 fs, as shown in Fig. 2. The beam diameter on the plate was approximately 1 mm, from the initial 12 mm output from the laser system. A total of -90 fs^2 of group delay dispersion was used to compress the pulse after the first stage.

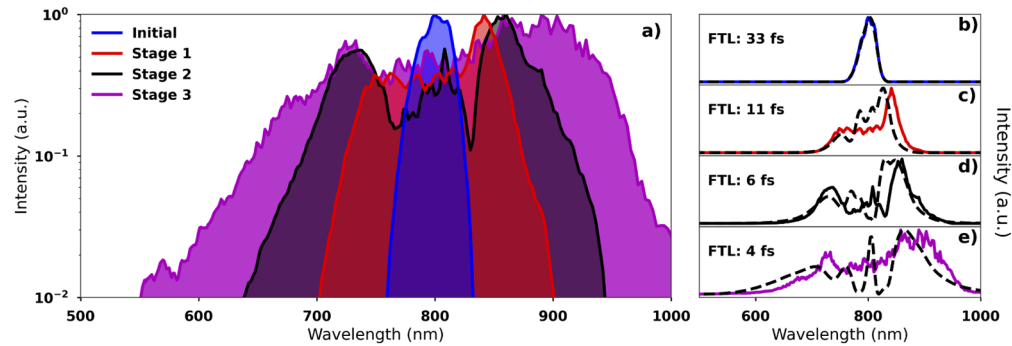


Fig. 2. Experimental and simulated spectra a) Experimental spectral measurements of the pulse with a varying number of stages in logarithmic scale. The initial pulse (blue) has a -20 dB width of 70 nm. The output bandwidth of each stage is 198 nm for a single stage (red), 316 nm for two stages (black), and 477 nm for three stages (magenta), leading to a total broadening factor of 6.8. b-e) Output spectrum for each stage experimentally (solid lines) and simulated (dashed) in linear scale. The experimental Fourier transform limit is listed for each stage. The simulated spectrum results in Fourier transform limits of 35 fs initially, 12 fs for 1 stage, 6 fs for 2 stages, and 4 fs for 3 stages.

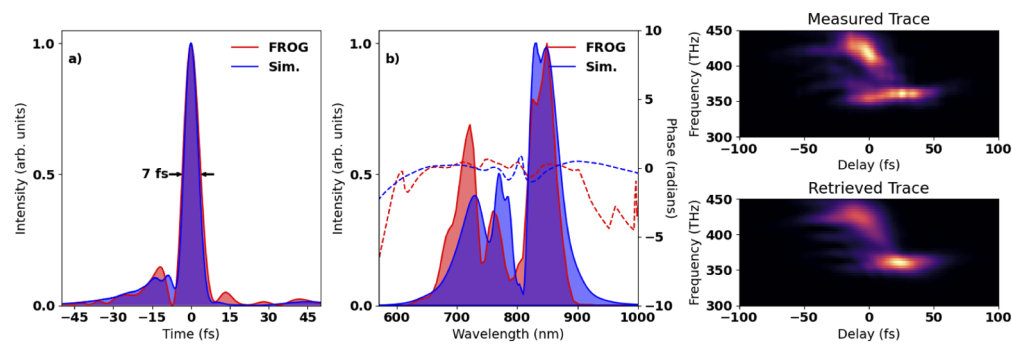


Fig. 3. TG-FROG reconstruction a) Temporal profile of two stage laser pulse from TG-FROG measurement (red) demonstrating a pulse duration of 7 fs (2-3 cycles); and from numerical simulations (blue) demonstrating an identical pulse duration of 7 fs. b) Spectrum of the two stage output, with power spectrum (solid) and spectral phase (dashed) overlaid. The reconstructed pulse (red) and the numerical simulations (blue) show good agreement. c-d) The experimentally measured and retrieved FROG traces.

3.3. Multi-staged compression

We implemented two additional stages experimentally, again with each stage consisting of a one to one telescope, a 0.5 mm fused silica plate, and chirped mirrors. Due to the temporal compression from the previous stages, it was necessary to increase the on-target beam diameter for each successive stage to maintain the correct intensity and not damage the fused silica. Beam diameters were approximately 1.7 mm and 1.9 mm in the second and third stage, respectively.

The second stage produces a spectrum which is broadened to a -20 dB width of 316 nm as shown in Fig. 2. Dispersion was corrected with a combination of -54 fs² from a chirped mirror and 22 fs² of dispersion from material dispersion from an additional plate of fused silica. When removing the dispersion accumulated propagating to the FROG, a retrieved pulse duration of 7 fs was measured, nearly at the transform limit of 6 fs as shown in Fig. 3.

In the third stage, the spectrum was further broadened to a -20 dB width of 477 nm, corresponding to a 4 fs FTL pulse duration or a sub-two cycle pulse. However, this spectrum was broader than the available chirped mirror bandwidth so compression could not occur. Simulations of the pulse predicted that the pulse should still be compressible to the FTL with GDD compensation. Similar to the prior stages, the phase is dominated by group velocity dispersion and thus is suitable for compression via chirped mirrors. For such large bandwidths, imperfect compensation of the GDD from the previous stage can have a significant effect on the broadening of the pulse. For the input of the third stage, an error in dispersion compensation of 22fs² produces a spectrum that is $\sim 15\%$ narrower.

The input energy of the two stage compressor was increased to 6.9 mJ. The beam diameter was increased to 24 mm to prevent optical damage after the first stage of compression. The fused silica plates were adjusted longitudinally to maintain approximately the same peak intensity on the fused silica as for the 0.95 mJ case. The spectra from the 6.9 mJ with two stages of broadening had a nearly identical output spectrum, with a FTL pulse duration of 8 fs, with spectral differences resulting from the additional nonlinearity propagating to the compressor. Simulations for the 6.9 mJ spectrum predict a 8.5 fs FTL. We were unable to compress the output of the two stages compression as the increased intensity required a beam diameter larger than our available chirped mirrors.

3.4. Focal spot characterization

The collimated, unbroadened beam is used to align the focal spot diagnostic and as a reference focal spot. When sent into the focal spot diagnostic, the unbroadened beam focused to a near diffraction limited spot of $2.1 \times 1.8 \pm 0.1 \mu\text{m}$ FWHM, as shown in Fig. 4(a). For the broadened case, a near identical focal spot of $2.1 \times 1.7 \pm 0.1 \mu\text{m}$ FWHM was measured, as shown in Fig. 4(b). The shape of the focus is largely maintained. A slight wing structure appears, resulting in the $1/e^2$ focal diameter to increase by $\sim 8\%$. The beam quality was largely similar at all wavelengths, with the $1/e^2$ width being within 10% of each other on average for each bandpass filter used. We observe a drop in peak fluence of only $\sim 7\%$ per stage, for two stages the peak was 15% lower, as shown in Fig. 4(c). Similarly, the energy contained in the $1/e^2$ focal spot for two stages decreased by $\approx 14\%$, as measured by a large area photodiode with a pinhole placed in the image plane and a thermopile power meter.

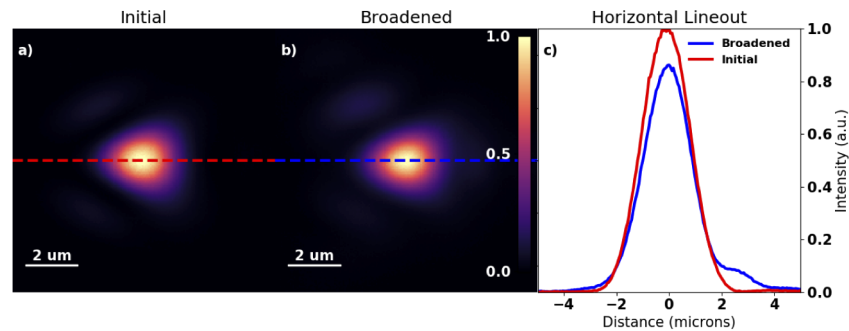


Fig. 4. Camera images of focal spot before and after pulse compression. a) Focal spot of the non-broadened laser pulse, normalized to the peak count values. b) Focal spot of the spectrally broadened laser pulse, normalized to the peak count value. c) Horizontal lineouts of the focal spots, normalized to the peak counts of the initial focal spot, show that the peak counts and enclosed energy drops by 15% while the overall shape is largely maintained, with only a slight additional wing structure added to the focus.

4. Strong and high field science applications

The two stage few-cycle output is suitable for a number of strong and high field applications. Due to the flexibility of the compression technique, we were able to use the same experimental setup that is discussed above for both regimes. Placing the fused silica on linear actuators enabled reliable positioning of the fused silica between input laser conditions.

4.1. Few-cycle HHG

We performed a high harmonic generation experiment with the compressed pulse, and measured the spectra using a homebuilt flat-field extreme ultraviolet (EUV) imaging spectrometer. The compressed 7 fs beam with roughly 0.7 mJ of focusable energy at a 1 kHz repetition rate was produced from the two stage compression setup. To compare the spectral broadening to the initial many-cycle pulse, the dielectric media were removed, enabling the 36 fs beam to be used traversing the same optics. The collimation optics of the compressor were adjusted such that the output was collimated for this case as well.

The laser was focused by a curved mirror with focal length of 50 cm onto a 256 micron Argon gas jet. The laser beam was apertured to an on-target intensity of $\sim 5 \times 10^{14} \text{ Wcm}^{-2}$, which produced the brightest harmonic emission for the many-cycle beam. The few-cycle beam had its energy further reduced to be as similar in intensity to the many-cycle as possible. Data was averaged for 20 seconds, consisting of 20,000 shots. The spectra produced by both the many-cycle and few-cycle beams are shown in Fig. 5. Compared to the many-cycle interaction, the few-cycle interaction produces a harmonic spectrum with significant broadening of the harmonics and a higher energy cutoff due to the dynamic phase matching from ionization [52,53]. The extra bandwidth at higher energies illuminates the aluminum absorption edge from the $1.4 \mu\text{m}$ Al x-ray filters used, demonstrating the source's potential for spectroscopic applications such as X-ray absorption fine structure [54]. On par with other experiments, the estimated flux of the beam exiting the gas jet is inferred to be $\sim 10^5$ photons/shot within the range of 38 to 43 eV [55,56] after accounting for filter absorption, the quantum efficiency of the x-ray CCD, and grating reflectivity.

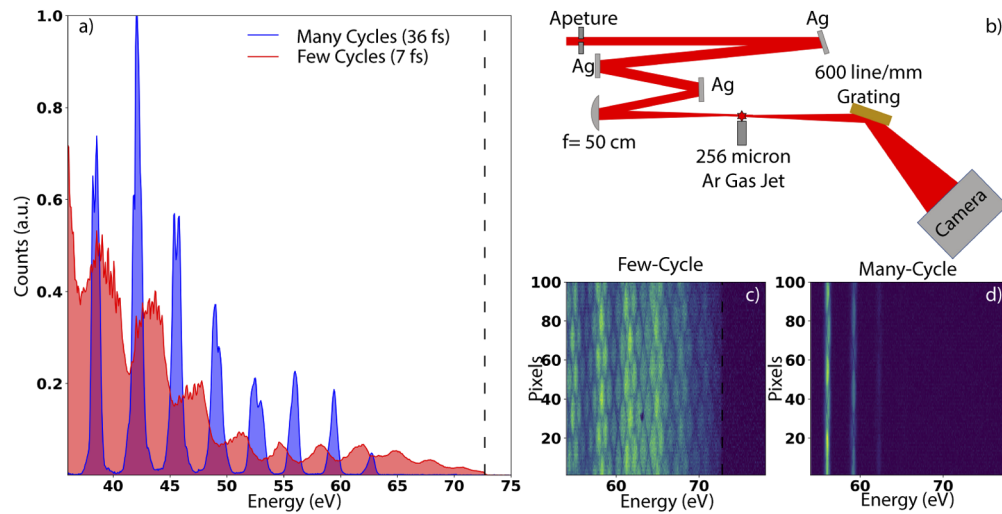


Fig. 5. Few-cycle EUV harmonic broadening **a)** EUV spectra produced through gas high harmonic generation, normalized to the maximum of the many-cycle spectrum. When driven by the many-cycle pulse (blue) discrete harmonics are observed. For the few-cycle pulse (red) broadening of the harmonic widths occurs. **b)** Diagram of the experimental setup used for gas high harmonic generation process. **c-d)** Images of the few-cycle and many-cycle spectra from 54 to 78 eV. The broadening of the harmonics in the few-cycle harmonic spectrum is able to resolve the sharp absorption edge of Al at 72 eV.

4.2. Relativistic electrons from a solid density target

Millijoule lasers can be focused to relativistic intensities on solid materials, producing suprathermal electron beams with a temperature that scales with laser intensity [57]. In order to have sufficient space to position a target at the laser focus, an OAP with a 50.8 mm focal length was used. The input beam was upcollimated to ~ 20 mm $1/e^2$ diameter using a reflective telescope to maintain a similar f-number as in the focal spot diagnostic. Due to the increase in collimated beam size, the fused silica plates were moved to maintain the same on-target intensity as was used in 3, similarly producing a measured few-cycle pulse duration of 7 fs. After compression, a gold-coated OAP focused the p-polarized beam onto a soda-lime glass target at an angle of incidence of 45° . The targets were mounted on a motorized XYZ translation stage to keep the target within the Rayleigh range of the laser and to continually refresh the target during the experiment. The electron spectra were then measured using a homebuilt permanent dipole magnet electron spectrometer positioned along the specular direction with the entrance slit of the spectrometer positioned ~ 12.5 cm from the laser focus. The dipole spectrometer was coupled to a scintillating screen (Lanex Fine) imaged by a digital camera (Basler). To ensure sufficient signal-to-noise, each electron spectrum was integrated over 650 shots.

For the comparison between many-cycle and few-cycle, we again removed the dielectric plates from the compressor and recollimated the many-cycle output. We performed experiments with three different beam parameters. Electron spectra were taken with the many-cycle pulse at two energies, 1 and 4 mJ. When compared to the few cycle pulse, this corresponds to a comparison case of having the same total energy (1 mJ) and having the same inferred peak intensity $1.3 \pm 0.1 \times 10^{18} \text{ W cm}^{-2}$, or 4 mJ. We then performed an intensity scan at these energies by changing the separation of the grating compressor of the laser system. The change of the inferred peak intensity due to the changing temporal profile was then modeled using the numerical techniques discussed in section 3. This takes into account the change in temporal

profile, including nonlinear propagation obtained while propagating into the vacuum chamber. This was done for the many-cycle and few-cycle laser beams. The same method for intensity scanning was used for all sets of data.

The spectra produced by the two highest intensities of the few-cycle and many-cycle drivers are shown in 6(a). While these pulses have approximately the same inferred peak intensity, the many-cycle pulse has approximately four times the laser energy. The temperature of the electrons measured scales with the intensity of the laser, as previously observed for many cycle pulse interactions [57]. The measured temperature of the compressed beam was 122 ± 6 keV with measured electron energies surpassing 1 MeV, comparable to what is measured with the many pulse beam at a similar intensity. Figure 6(b) shows the electron spectra of the many-cycle compared to the few-cycle when they have the same energy and inferred peak intensity. The maximum energy as a function of intensity is shown in Fig. 6(d). A clear difference can be observed between the few-cycle 1 mJ driver and the many-cycle 1 mJ driver, suggesting a much higher intensity in the former case. Additionally, as we reduce the intensity by introducing GDD, we observe the expected drop in the maximum electron energies.

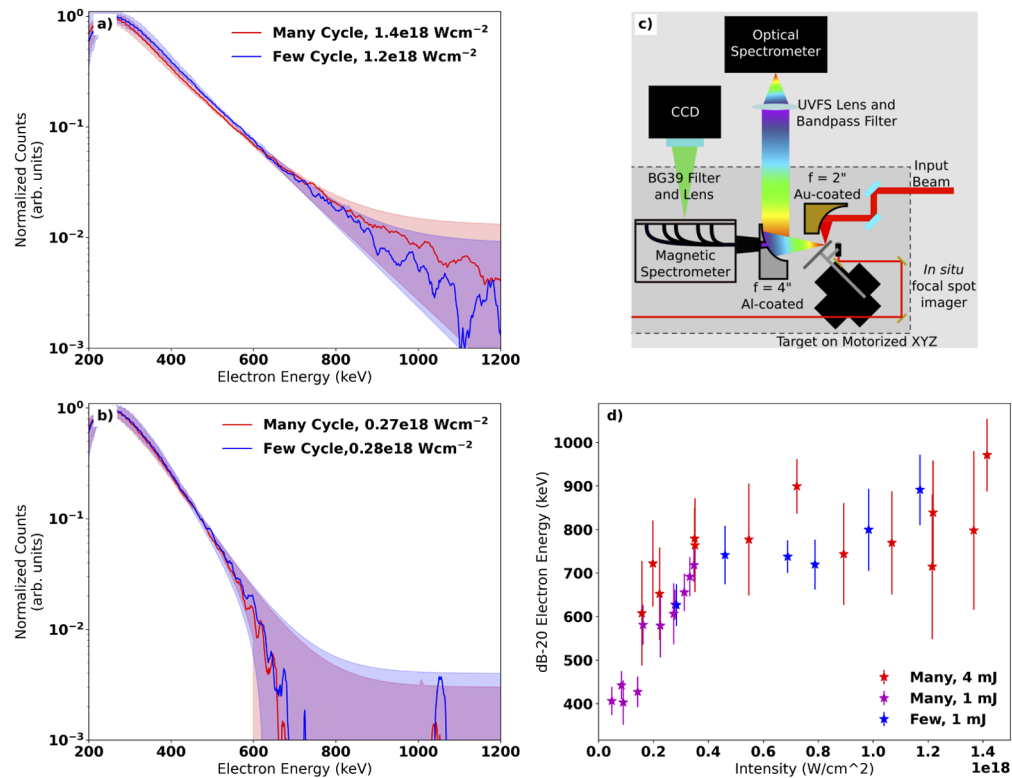


Fig. 6. Relativistic electron generation a) Electron spectrum produced by the few-cycle pulse and many-cycle pulse at intensities of $1.2 \times 10^{18} \text{ Wcm}^{-2}$ and $1.4 \times 10^{18} \text{ Wcm}^{-2}$. Electron energies above 1 MeV detected. b) Electron spectrum produced by the few-cycle pulse and many-cycle pulse at intensities of $0.27 \times 10^{18} \text{ Wcm}^{-2}$ and $0.28 \times 10^{18} \text{ Wcm}^{-2}$. c) Diagram of the experimental setup use for relativistic electron generation. d) Shows the change in electron energy at 1% the maximum electron spectrum amplitude as the laser compressor is adjusted, changing the peak intensities. Note that the intensities for the few cycle case are inferred.

5. Discussion

The amount of accumulated nonlinearity in the dielectric plate can be characterized with the B-integral:

$$B = \frac{2\pi}{\lambda_0} \int n_2 I(z) dz,$$

where λ_0 is the central wavelength of the laser, n_2 is the nonlinear index of the dielectric, and the intensity $I(z)$ is the maximum intensity of the pulse at location z inside of the material. Commonly, $I(z)$ is assumed to be constant throughout propagation, but as the bandwidth of the pulse increases this approximation becomes less valid. The B-integrals reported in this work are calculated using a summation approximation of the B-integral as it propagates inside of the material, based on the nonlinear simulations of the system. A B-integral of 3.6 was calculated for the first stage, 2.8 for the second stage, and 2.7 for the third stage. The total B-integral of 9.7 for all three stages, with the B integral being slightly higher due to the presence of nonlinearity from the air and vacuum window prior to the compressor. The FTL for the spectral output of each stage is predicted well by the simulations, and is also in agreement with analytical spectral broadening factor for a Gaussian pulse [40].

Particularly in nonlinear schemes of pulse broadening, great care must be taken when discussing the properties of the beam. There is likely some amount of inhomogeneity in the beam profile with regards to both broadening and pulse duration. For instance, in the case of TFC, our 12 mm beam entering a dielectric at a lower B integral [47] produces narrower spectra, but also produces spatial phase errors that can not easily be compensated [40]. We have previously observed in our laser system that there exist significant losses in the focal spot quality and intensity when a TFC geometry is used [40,47]. These losses appeared to have been mitigated in the system utilized in this paper. The mechanism for why the focusability of the beam has improved over the collimated system cannot be explained using the same models and warrants further study. One potential explanation is the interaction between the multiple stages of spectral broadening in a focusing geometry and nonlinear lensing occurring inside of the dielectric media.

While the spatiotemporal effects do not introduce substantial losses in the focusability of the pulse, they introduce complications into a calculation of the peak intensity of the laser [40,58]. Assuming the focal spots and pulse durations discussed in this work, the intensity could increase by a factor of ~ 1.2 to ~ 3.7 [40]. The peak intensity was not directly measured, and with spatially averaging measurements we can only infer an intensity value, which may vary between a value of 0.4 and $1.2 \times 10^{18} \text{ Wcm}^{-2}$. The relativistic electron spectra produced by the compressed few-cycle laser pulse was nearly identical to the many-cycle laser pulse with an on-target intensity of $1.4 \times 10^{18} \text{ Wcm}^{-2}$, shown in Fig. 6(a), suggesting that we are likely closer to the higher estimated intensity. When the intensity scan was performed, pulses with similar inferred peak intensities produce similar electron spectra, as seen in Figs. 6(b) and 6(d). Though factors such as laser contrast, pulse duration, pulse structure, and focal quality may have an unknown impact in this experiment, the similarities between the two experiments suggest that these effects are minimal.

The pulse compression scheme presented in this work used all commercially available components with a total cost of less than three thousand US dollars, yet enabled MeV electrons to be generated with a factor of 4 less laser energy. While the system does require to be under vacuum, potentially increasing the cost, relativistic laser-plasma experiments require the use of vacuum, and such a system may be implemented within current vacuum infrastructure in a manner similar to ours. The current dominant cost is due to the chirped mirrors. Increasing the energy of the laser system to even 10 mJ will require 2 inch optics to maintain a collimated intensity below 0.5 TWcm^{-2} after 2 stages of compression, corresponding to chirped mirrors which can cost tens of thousands of dollars.

With the required high reflectivity dielectric optics, terawatt peak powers are possible out of our laser system, a commercially available single-stage amplifier. This scheme can be easily adapted for laser systems with tens of millijoules, such as the 30 mJ red Wyvern (KMLabs). Assuming similar losses to what we have observed in our system, a two stage compressor with larger diameter optics, and a F/1.5 OAP focusing optic enables the commercially available Red Wyvern to achieve on-target intensities of $\sim 10^{20}$ Wcm⁻² at a kilohertz repetition rate. At such high intensities laser contrast is an important consideration. The ratio between laser prepulse and the on-target intensity laser is known as the laser contrast. Laser contrast has been shown to have a major impact in experiments such as laser ion acceleration and high harmonic generation [59,60]. Changing the laser contrast by changing the main pulse intensity does not necessarily imply that the prepulse is negligible, and in some experiments pulse cleaning may be required. It should be noted that since the laser system used is not Carrier Envelope Phase stabilized, the compressed pulse would not be either. If applied to systems that are Carrier Envelope Phase stabilized or have features such as orbital angular momentum these features should be maintained [32,61].

In this Article, relativistically intense few-cycle laser pulses capable of driving both high and strong field physics were demonstrated utilizing an inexpensive and easy to implement staged compression setup. In hollow core fiber compression, the laser undergoes SPM in a gas media and the broadened portion of the beam propagates through a waveguide, maintaining beam quality. In multiple plate compression, the technique is similar, now the SPM media is a solid dielectric and the waveguiding comes in the form of the repeating nonlinear lens. Our technique can be thought of in a similar manner, where instead of using the nonlinear lens to guide the broadened spectra we instead use repeated real lenses, in the form of our reflective curved mirrors. The benefit of such an approach is that we decouple the SPM from the recollimation, enabling more compact and efficient geometries to be employed. Due to this technique relying only on self-phase modulation and dispersion compensation, it is expected that this technique can be applied to other optical and near infrared wavelengths. Additionally, if a dielectric material is chosen with a similar nonlinear index and is transparent across the entire range of expected spectra this technique should work.

Funding. National Science Foundation (DGE-1633631, DMR-1548924, PHY-1753165).

Acknowledgments. This work was supported by STROBE: A National Science Foundation Science & Technology Center under Grant No. DMR-1548924. This material is based upon work supported by the National Science Foundation under the CAREER program Grant No. PHY-1753165, and under grant number DGE-1633631.

Disclosures. F.D. and M.S.: University of California, Irvine (P)

A provisional patent application has been filed under the authors M.S. and F.D. based on the results of this paper.

Data availability. The data from this work is available from the corresponding author upon reasonable request.

References

1. D. Strickland and G. Mourou, "Compression of amplified chirped optical pulses," *Opt. Commun.* **56**(3), 219–221 (1985).
2. J. W. Yoon, C. Jeon, J. Shin, S. K. Lee, H. W. Lee, I. W. Choi, H. T. Kim, J. H. Sung, and C. H. Nam, "Achieving the laser intensity of 5.5×10^{22} w/cm² with a wavefront-corrected multi-PW laser," *Opt. Express* **27**(15), 20412–20420 (2019).
3. T. Tajima and J. M. Dawson, "Laser electron accelerator," *Phys. Rev. Lett.* **43**(4), 267–270 (1979).
4. J. Faure, Y. Glinec, A. Pukhov, S. Kiselev, S. Gordienko, E. Lefebvre, J.-P. Rousseau, F. Burgy, and V. Malka, "A laser-plasma accelerator producing monoenergetic electron beams," *Nature* **431**(7008), 541–544 (2004).
5. S. P. D. Mangles, C. D. Murphy, Z. Najmudin, A. G. R. Thomas, J. L. Collier, A. E. Dangor, E. J. Divall, P. S. Foster, J. G. Gallacher, C. J. Hooker, D. A. Jaroszynski, A. J. Langley, W. B. Mori, P. A. Norreys, F. S. Tsung, R. Viskup, B. R. Walton, and K. Krushelnick, "Monoenergetic beams of relativistic electrons from intense laser-plasma interactions," *Nature* **431**(7008), 535–538 (2004).
6. C. G. R. Geddes, C. Toth, J. van Tilborg, E. Esarey, C. B. Schroeder, D. Bruhwiler, C. Nieter, J. Cary, and W. P. Leemans, "High-quality electron beams from a laser wakefield accelerator using plasma-channel guiding," *Nature* **431**(7008), 538–541 (2004).

7. F. Albert, S. G. Anderson, D. J. Gibson, C. A. Hagmann, M. S. Johnson, M. Messerly, V. Semenov, M. Y. Shverdin, B. Rusnak, A. M. Tremaine, F. V. Hartemann, C. W. Siders, D. P. McNabb, and C. P. J. Barty, "Characterization and applications of a tunable, laser-based, mev-class compton-scattering γ -ray source," *Phys. Rev. Spec. Top.-Accel. Beams* **13**(7), 070704 (2010).
8. S. Chen, N. D. Powers, I. Ghebregziabher, C. M. Maharjan, C. Liu, G. Golovin, S. Banerjee, J. Zhang, N. Cunningham, A. Moorti, S. Clarke, S. Pozzi, and D. P. Umstadter, "MeV-Energy X Rays from Inverse Compton Scattering with Laser-Wakefield Accelerated Electrons," *Phys. Rev. Lett.* **110**(15), 155003 (2013).
9. M. L. Zhou, X. Q. Yan, G. Mourou, J. A. Wheeler, J. H. Bin, J. Schreiber, and T. Tajima, "Proton acceleration by single-cycle laser pulses offers a novel monoenergetic and stable operating regime," *Phys. Plasmas* **23**(4), 043112 (2016).
10. D. Guénot, D. Gustas, A. Vernier, B. Beaurepaire, F. Böhle, M. Bocoum, M. Lozano, A. Jullien, R. Lopez-Martens, A. Lifschitz, and J. Faure, "Relativistic electron beams driven by kHz single-cycle light pulses," *Nat. Photonics* **11**(5), 293–296 (2017).
11. D. Gustas, D. Guénot, A. Vernier, S. Dutt, F. Böhle, R. Lopez-Martens, A. Lifschitz, and J. Faure, "High-charge relativistic electron bunches from a khz laser-plasma accelerator," *Phys. Rev. Accel. Beams* **21**(1), 013401 (2018).
12. F. Salehi, M. Le, L. Railing, and H. M. Milchberg, "Laser-accelerated, low divergence 15 mev quasi-monoenergetic electron bunches at 1 khz," (2020).
13. B. Beaurepaire, A. Lifschitz, and J. Faure, "Electron acceleration in sub-relativistic wakefields driven by few-cycle laser pulses," *New J. Phys.* **16**(2), 023023 (2014).
14. M. Ouillé, A. Vernier, F. Böhle, M. Bocoum, A. Jullien, M. Lozano, J.-P. Rousseau, Z. Cheng, D. Gustas, A. Blumenstein, P. Simon, S. Haessler, J. Faure, T. Nagy, and R. Lopez-Martens, "Relativistic-intensity near-single-cycle light waveforms at khz repetition rate," *Light: Sci. Appl.* **9**(1), 47 (2020).
15. N. M. Naumova, J. A. Nees, I. V. Sokolov, B. Hou, and G. A. Mourou, "Relativistic generation of isolated attosecond pulses in a λ^3 focal volume," *Phys. Rev. Lett.* **92**(6), 063902 (2004).
16. P. Heissler, R. Hörlein, J. M. Mikhailova, L. Waldecker, P. Tzallas, A. Buck, K. Schmid, C. M. S. Sears, F. Krausz, L. Veisz, M. Zepf, and G. D. Tsakiris, "Few-cycle driven relativistically oscillating plasma mirrors: A source of intense isolated attosecond pulses," *Phys. Rev. Lett.* **108**(23), 235003 (2012).
17. R. H. Stolen and C. Lin, "Self-phase-modulation in silica optical fibers," *Phys. Rev. A* **17**(4), 1448–1453 (1978).
18. C. V. Shank, R. L. Fork, R. Yen, R. H. Stolen, and W. J. Tomlinson, "Compression of femtosecond optical pulses," *Appl. Phys. Lett.* **40**(9), 761–763 (1982).
19. A. A. Mak, L. N. Soms, V. A. Fromzel', and V. E. Iashin, "Nd-glass lasers," Moscow Izdatel Nauka (1990).
20. M. Kaumanns, V. Pervak, D. Kormin, V. Leshchenko, A. Kessel, M. Ueffing, Y. Chen, and T. Nubbemeyer, "Multipass spectral broadening of 18 mJ pulses compressible from 1.3 ps to 41 fs," *Opt. Lett.* **43**(23), 5877–5880 (2018).
21. M. Ueffing, S. Reiger, M. Kaumanns, V. Pervak, M. Trubetskov, T. Nubbemeyer, and F. Krausz, "Nonlinear pulse compression in a gas-filled multipass cell," *Opt. Lett.* **43**(9), 2070–2073 (2018).
22. T. Metzger, C. Grebing, C. Herkommer, S. Klingebiel, P. Krötz, S. Prinz, S. Stark, C. Y. Teisset, C. Wandt, and K. Michel, "High-power ultrafast industrial thin-disk lasers," in *Short-pulse High-energy Lasers and Ultrafast Optical Technologies*, vol. 11034 P. Bakule and C. L. Haefner, eds., International Society for Optics and Photonics (SPIE, 2019), pp. 64–71.
23. C. Rolland and P. B. Corkum, "Compression of high-power optical pulses," *J. Opt. Soc. Am. B* **5**(3), 641–647 (1988).
24. E. Mével, O. Tcherbakoff, F. Salin, and E. Constant, "Extracavity compression technique for high-energy femtosecond pulses," *J. Opt. Soc. Am. B* **20**(1), 105–108 (2003).
25. M. Hemmer, M. Baudisch, A. Thai, A. Couairon, and J. Biegert, "Self-compression to sub-3-cycle duration of mid-infrared optical pulses in dielectrics," *Opt. Express* **21**(23), 28095–28102 (2013).
26. M. Seidel, G. Arisholm, J. Brons, V. Pervak, and O. Pronin, "All solid-state spectral broadening: an average and peak power scalable method for compression of ultrashort pulses," *Opt. Express* **24**(9), 9412–9428 (2016).
27. M. Nisoli, S. Stagira, S. De Silvestri, O. Svelto, S. Sartania, Z. Cheng, M. Lenzner, C. Spielmann, and F. Krausz, "A novel-high energy pulse compression system: generation of multigigawatt sub-5-fs pulses," *Appl. Phys. B* **65**(2), 189–196 (1997).
28. T. Nagy, S. Hädrich, P. Simon, A. Blumenstein, N. Walther, R. Klas, J. Buldt, H. Stark, S. Breitkopf, P. Jójárt, I. Seres, Z. Várallyay, T. Eidam, and J. Limpert, "Generation of three-cycle multi-millijoule laser pulses at 318 w average power," *Optica* **6**(11), 1423–1424 (2019).
29. T. Nagy, M. Kretschmar, M. J. J. Vrakking, and A. Rouzée, "Generation of above-terawatt 1.5-cycle visible pulses at 1 khz by post-compression in a hollow fiber," *Opt. Lett.* **45**(12), 3313–3316 (2020).
30. G. Fan, P. A. Carpeggiani, Z. Tao, E. Kaksis, T. Balciunast, G. Coccia, V. Cardin, F. Légaré, B. E. Schmidt, and A. Baltuška, "TW-Peak-Power Post-Compression of 70-mJ pulses from an Yb amplifier," in *2019 Conference on Lasers and Electro-Optics (CLEO)*, (2019), pp. 1–2.
31. S. Bohman, A. Suda, T. Kanai, S. Yamaguchi, and K. Midorikawa, "Generation of 5.0fs, 5.0mj pulses at 1khz using hollow-fiber pulse compression," *Opt. Lett.* **35**(11), 1887–1889 (2010).
32. S. Carbajo, E. Granados, D. Schimpf, A. Sell, K.-H. Hong, J. Moses, and F. X. Kärtner, "Efficient generation of ultra-intense few-cycle radially polarized laser pulses," *Opt. Lett.* **39**(8), 2487–2490 (2014).
33. C.-H. Lu, Y.-J. Tsou, H.-Y. Chen, B.-H. Chen, Y.-C. Cheng, S.-D. Yang, M.-C. Chen, C.-C. Hsu, and A. H. Kung, "Generation of intense supercontinuum in condensed media," *Optica* **1**(6), 400 (2014).

34. C.-H. Lu, T. Witting, A. Husakou, M. J. Vrakking, A. H. Kung, and F. J. Furch, "Sub-4 fs laser pulses at high average power and high repetition rate from an all-solid-state setup," *Opt. Express* **26**(7), 8941–8956 (2018).
35. P. He, Y. Liu, K. Zhao, H. Teng, X. He, P. Huang, H. Huang, S. Zhong, Y. Jiang, S. Fang, X. Hou, and Z. Wei, "High-efficiency supercontinuum generation in solid thin plates at 0.1 TW level," *Opt. Lett.* **42**(3), 474–477 (2017).
36. G. Mourou, S. Mironov, E. Khazanov, and A. Sergeev, "Single cycle thin film compressor opening the door to Zeptosecond-Exawatt physics," *Eur. Phys. J. Spec. Top.* **223**(6), 1181–1188 (2014).
37. C. Radier, G. Mourou and G. Cheriaux, "Device for generating a short duration laser pulse U.S. patent20110299152a1,".
38. M. Masruri, J. Wheeler, J. Wheeler, I. Dancus, R. Fabbri, A. Nazîru, R. Secareanu, D. Ursescu, G. Cojocaru, R. Ungureanu, D. Farinella, M. Pittman, S. Mironov, S. Balascuta, D. Doria, D. Ros, and R. Dabu, "Optical Thin Film Compression for Laser Induced Plasma Diagnostics," in *Conference on Lasers and Electro-Optics (2019), paper SW4E.3*, (Optical Society of America, 2019), p. SW4E.3.
39. S. Y. Mironov, S. Fourmaux, P. Lassonde, V. Ginzburg, S. Payeur, J.-C. Kieffer, E. Khazanov, and G. Mourou, "Thin plate compression of a sub-petawatt ti: Sa laser pulses," *Appl. Phys. Lett.* **116**(24), 241101 (2020).
40. E. A. Khazanov, S. Y. Mironov, and G. A. Mourou, "Nonlinear compression of high-power laser pulses: compression after compressor approach," *Phys.-Usp.* **62**(11), 1096–1124 (2019).
41. D. M. Farinella, J. Wheeler, A. E. Hussein, J. Nees, M. Stanfield, N. Beier, Y. Ma, G. Cojocaru, R. Ungureanu, M. Pittman, J. Demailly, E. Baynard, R. Fabbri, M. Masruri, R. Secareanu, A. Naziru, R. Dabu, A. Maksimchuk, K. Krushelnick, D. Ros, G. Mourou, T. Tajima, and F. Dollar, "Focusability of laser pulses at petawatt transport intensities in thin-film compression," *J. Opt. Soc. Am. B* **36**(2), A28–A32 (2019).
42. S. Y. Mironov, J. Wheeler, R. Gonin, G. Cojocaru, R. Ungureanu, R. Banici, M. Serbanescu, R. Dabu, G. Mourou, and E. A. Khazanov, "100 j-level pulse compression for peak power enhancement," *Quantum Electron.* **47**(3), 173–178 (2017).
43. V. N. Ginzburg, A. A. Kochetkov, I. V. Yakovlev, S. Y. Mironov, A. A. Shaykin, and E. A. Khazanov, "Influence of the cubic spectral phase of high-power laser pulses on their self-phase modulation," *Quantum Electron.* **46**(2), 106–108 (2016).
44. S. Mironov, P. Lassonde, J.-C. Kieffer, E. Khazanov, and G. Mourou, "Spatially-uniform temporal recompression of intense femtosecond optical pulses," *Eur. Phys. J. Spec. Top.* **223**(6), 1175–1180 (2014).
45. V. N. Ginzburg, I. V. Yakovlev, A. S. Zuev, A. P. Korobeynikova, A. A. Kochetkov, A. A. Kuźmin, S. Y. Mironov, A. A. Shaykin, I. A. Shaykin, and E. A. Khazanov, "Compression after compressor: threefold shortening of 200-TW laser pulses," *Quantum Electron.* **49**(4), 299–301 (2019).
46. V. Ginzburg, I. Yakovlev, A. Zuev, A. Korobeynikova, A. Kochetkov, A. Kuzmin, S. Mironov, A. Shaykin, I. Shaikin, E. Khazanov, and G. Mourou, "Fivefold compression of 250-tw laser pulses," *Phys. Rev. A* **101**(1), 013829 (2020).
47. D. M. Farinella, M. Stanfield, N. Beier, T. Nguyen, S. Hakimi, T. Tajima, F. Dollar, J. Wheeler, and G. Mourou, "Demonstration of thin film compression for short-pulse x-ray generation," *Int. J. Mod. Phys. A* **34**(34), 1943015 (2019).
48. V. N. Ginzburg, I. V. Yakovlev, A. S. Zuev, A. P. Korobeynikova, A. A. Kochetkov, A. A. Kuzmin, S. Y. Mironov, A. A. Shaykin, I. A. Shaikin, and E. A. Khazanov, "Two-stage nonlinear compression of high-power femtosecond laser pulses," *Quantum Electron.* **50**(4), 331–334 (2020).
49. S. Mironov, V. Lozhkarev, G. Luchinin, A. Shaykin, and E. Khazanov, "Suppression of small-scale self-focusing of high-intensity femtosecond radiation," *Appl. Phys. B* **113**(1), 147–151 (2013).
50. G. Ycas, D. Maser, and D. Hickstein, "Pynlo: Nonlinear optics modelling for python," <https://pynlo.readthedocs.io/en/latest/> (2015).
51. J. Hult, "A fourth-order runge–kutta in the interaction picture method for simulating supercontinuum generation in optical fibers," *J. Lightwave Technol.* **25**(12), 3770–3775 (2007).
52. C. Spielmann, "Generation of coherent x-rays in the water window using 5-femtosecond laser pulses," *Science* **278**(5338), 661–664 (1997).
53. J. Seres, P. Wobrauschek, C. Strelî, V. S. Yakovlev, E. Seres, F. Krausz, and C. Spielmann, "Generation of coherent keV x-rays with intense femtosecond laser pulses," *New J. Phys.* **8**(10), 251 (2006).
54. D. Popmintchev, B. R. Galloway, M.-C. Chen, F. Dollar, C. A. Mancuso, A. Hankla, L. Miaja-Avila, G. O'Neil, J. M. Shaw, G. Fan, S. Ališauskas, G. Andriukaitis, T. Balčiunas, O. D. Mücke, A. Pugzlys, A. Baltuška, H. C. Kapteyn, T. Popmintchev, and M. M. Murnane, "Near- and extended-edge x-ray-absorption fine-structure spectroscopy using ultrafast coherent high-order harmonic supercontinua," *Phys. Rev. Lett.* **120**(9), 093002 (2018).
55. P. C. Huang, C. H. Lu, B. H. Chen, S. D. Yang, M.-C. Chen, and A. H. Kung, "Euv continuum from compressed multiple thin plate supercontinuum," in *Conference on Lasers and Electro-Optics*, (Optical Society of America, 2016), p. FTu3N.7.
56. M. Stanfield, H. Allison, N. Beier, S. Hakimi, A. E. Hussein, and F. Dollar, "Few cycle euv continuum generation via thin film compression," in *2020 Conference on Lasers and Electro-Optics (CLEO)*, (2020), pp. FF2C–7.
57. A. G. Mordovanakis, P.-E. Masson-Laborde, J. Easter, K. Popov, B. Hou, G. Mourou, W. Rozmus, M. G. Haines, J. Nees, and K. Krushelnick, "Temperature scaling of hot electrons produced by a tightly focused relativistic-intensity laser at 0.5 khz repetition rate," *Appl. Phys. Lett.* **96**(7), 071109 (2010).
58. E. Perevezentsev, A. Poteomkin, and E. Khazanov, "Comparison of phase-aberrated laser beam quality criteria," *Appl. Opt.* **46**(5), 774–784 (2007).

59. M. Kaluza, J. Schreiber, M. I. K. Santala, G. D. Tsakiris, K. Eidmann, J. Meyer-ter Vehn, and K. J. Witte, "Influence of the laser prepulse on proton acceleration in thin-foil experiments," *Phys. Rev. Lett.* **93**(4), 045003 (2004).
60. F. Dollar, P. Cummings, V. Chvykov, L. Willingale, M. Vargas, V. Yanovsky, C. Zolick, A. Maksimchuk, A. G. R. Thomas, and K. Krushelnick, "Scaling high-order harmonic generation from laser-solid interactions to ultrahigh intensity," *Phys. Rev. Lett.* **110**(17), 175002 (2013).
61. F. Kong, H. Larocque, E. Karimi, P. B. Corkum, and C. Zhang, "Generating few-cycle radially polarized pulses," *Optica* **6**(2), 160 (2019).